Journal of the American College of Cardiology
© 2006 by the American College of Cardiology Foundation
Published by Elsevier Inc.

Vol. 48, No. 10, 2006
ISSN 0735-1097/06/$32.00
doi:10.1016/j.jacc.2006.08.029

Noninvasive Characterization of Myocardial Molecular Interventions by Integrated Positron Emission Tomography and Computed Tomography

Bettina Wagner, DVM,* Martina Anton, PHD,† Stephan G. Nekolla, PHD,* Sybille Reder, MT,* Julia Henke, DVM,† Stefan Seidl, MD,‡ Renate Hegenloh, MT,§ Masao Miyagawa, MD,* Roland Haubner, PHD,* Markus Schwaiger, MD,* Frank M. Bengel, MD*‖

Munich, Germany; and Baltimore, Maryland

OBJECTIVES We sought to investigate the usefulness of integrated positron emission tomography (PET) and computed tomography (CT) for in vivo characterization of an angiogenesis-directed molecular intervention.

BACKGROUND Controversies about the effectiveness of molecular therapies for cardiovascular disease have prompted the need for more powerful noninvasive imaging techniques.

METHODS In a model of regional adenoviral transfer of the $VEGF_{121}$ gene to myocardium of healthy pigs, PET-CT using multiple molecular-directed radiotracers was employed.

RESULTS Two days after gene transfer, successful transgene expression was noninvasively confirmed by a reporter probe targeting co-expressed HSV1-sr39tk reporter gene. The CT-derived ventricular function and morphology remained unaltered (left ventricular ejection fraction 57 ± 5% in adenovirus-injected animals vs. 53 ± 5% in controls; $p = 0.36$). Increased regional perfusion was identified in areas overexpressing VEGF (myocardial blood flow during adenosine-induced vasodilation 1.47 ± 0.49 vs. 1.14 ± 0.27 ml/g/min in remote areas; $p = 0.01$), corroborating in vivo effects on microvascular tone and permeability. Finally, regional angiogenesis-associated $\alpha_v\beta_3$ integrin expression was not enhanced, suggesting little contribution to the perfusion increase. Fusion of CT morphology and tracer-derived molecular signals allowed for accurate regional localization of biologic signals. Findings were validated by control vectors, sham-operated animals, and ex vivo tissue analysis.

CONCLUSIONS Integrated PET-CT has the potential to dissect cardiovascular biologic mechanisms from gene expression to physiologic function and morphology. The VEGF overexpression in healthy myocardium increases myocardial perfusion without significant up-regulation of $\alpha_v\beta_3$ integrin adhesion molecules early after the intervention. (J Am Coll Cardiol 2006;48: 2107–15) © 2006 by the American College of Cardiology Foundation

Various gene- and cell-based molecular therapeutic approaches directed against cardiovascular disease have been evaluated in experimental settings, and some have reached the stage of clinical trials (1,2). Despite rapid progress, some basic principles of these therapies are still under development, and issues related to therapeutic efficacy and the best delivery of agents to myocardium are still debated. For example, early experimental results for angiogenesis therapy of myocardial ischemia were difficult to reproduce in the clinical setting (3,4).

These developments have prompted a need for powerful noninvasive imaging tools to provide specific disease-related biologic insights and facilitate the translation from experimental to clinical practice. A single cardiac imaging modality for in vivo characterization of tissue biology, physiologic function, and morphologic appearance could thus be of considerable value.

In the present study, we explored the potential of integrated positron emission tomography (PET) and computed tomography (CT) for noninvasive imaging of a myocardial molecular intervention (i.e., the regional transfer of vascular endothelial growth factor [VEGF] gene to myocardium of healthy pigs). Our primary goal was to study the feasibility of this methodology for integrated imaging of the heart from its morphology to subcellular function. As a secondary goal, we intended to get further insights into the effects of VEGF overexpression on the tissue level and on the heart as a whole.

METHODS

Experimental protocol. The experimental protocol was approved by the regional governmental commission of animal protection (Regierung von Oberbayern) and is summarized in Table 1.

Eleven young domestic pigs (30 to 40 kg; Versuchsstation, Thalhausen, Germany) underwent left thoracotomy under anesthesia with mechanical ventilation (10 mg/kg/h

From the *Nuklearmedizinische Klinik und Poliklinik, †Institut für Experimentelle Onkologie und Therapieforschung, ‡Institut für Allgemeine Pathologie und Pathologische Anatomie, and §Abteilung für Gefäßchirurgie, Technische Universität München, Germany; and the ‖Division of Nuclear Medicine, Johns Hopkins University, Baltimore, Maryland. Supported by a grant from the Deutsche Forschungsgemeinschaft (Be 2217/4-1).

Manuscript received July 31, 2006, accepted August 30, 2006.

JACC Vol. 48, No. 10, 2006
November 21, 2006:2107–15

Abbreviations and Acronyms

Ad_{sr39tk}	= replication defective type 5 adenovirus expressing a mutant herpesviral thymidine kinase reporter gene
$Ad_{Tk\text{-}VEGF}$	= replication defective type 5 adenovirus co-expressing a mutant herpesviral thymidine kinase reporter gene and the human $VEGF_{121}$ gene
Ad_{VEGF}	= replication defective type 5 adenovirus expressing the human $VEGF_{121}$ gene
CT	= computed tomography
FHBG	= [^{18}F]fluoro-hydroxymethylbutyl-guanine
MBF	= myocardial blood flow
PET	= positron emission tomography
VEGF	= vascular endothelial growth factor

propofol intravenously, fentanyl intravenously as required). Pericardium was opened, and gene transfer was performed in study group animals (n = 8) using doses of 1×10^{10} plaque-forming units (pfu) of adenovirus (total volume 1 ml, aliquoted into 5 syringes). Those were consecutively injected into 2 separate myocardial areas of approximately 2 × 2 cm. Control group animals (n = 3) received saline injection following the same protocol. Both injection sites were marked with titanium clips (LIGACLIP 20/20, Ethicon, Norderstedt, Germany).

Two days later, all pigs were anesthetized using the same regimen and underwent PET-CT. Animals were killed after imaging (60 mg/kg sodium pentobarbital intravenously). Hearts were excised and rinsed, and transmural tissue samples were taken from the 2 areas of injection and from a remote area (inferior wall).

Table 1. Animals and Study Protocol

	LV Myocardial Injection Site		
Animal	Basal Anterior	Distal Anterolateral	PET-CT Protocol
1	$Ad_{Tk\text{-}VEGF}$	Ad_{sr39tk}	Study group, day 2
2	Ad_{sr39tk}	$Ad_{Tk\text{-}VEGF}$	Contrast enhanced CT
3	$Ad_{Tk\text{-}VEGF}$	Ad_{VEGF}	2× [^{13}N]-ammonia perfusion PET
4	Ad_{VEGF}	$Ad_{Tk\text{-}VEGF}$	[^{18}F]-FHBG reporter gene PET
5	$Ad_{Tk\text{-}VEGF}$	Ad_{sr39tk}	2nd session (animals 5–8, day 3–9)
6	Ad_{sr39tk}	$Ad_{Tk\text{-}VEGF}$	Contrast enhanced CT
7	$Ad_{Tk\text{-}VEGF}$	Ad_{VEGF}	[^{13}N]-ammonia perfusion PET
8	Ad_{VEGF}	$Ad_{Tk\text{-}VEGF}$	[^{18}F]-galacto-RGD PET
9	Saline	Saline	Control group, day 2
10	Saline	Saline	Contrast enhanced CT
11	Saline	Saline	2× [^{13}N]-ammonia perfusion PET

Ad_{sr39tk} = adenovirus expressing mutant herpesviral thymidine kinase reporter gene; $Ad_{Tk\text{-}VEGF}$ = adenovirus coexpressing mutant herpesviral thymidine kinase reporter gene and vascular endothelial growth factor 121 gene; Ad_{VEGF} = adenovirus expressing vascular endothelial growth factor 121 gene; CT = computed tomography; FHBG = fluoro-hydroxymethylbutyl-guanine; LV = left ventricular; PET = positron emission tomography.

Adenoviral vector preparation and injection. E1 region-deleted replication-deficient adenoviral vectors carrying transgenes under transcriptional control of human cytomegalovirus promoter were used. Vectors were double cesium chloride purified. Titers were determined by plaque assay on 293 cells. For monitoring of therapeutic gene expression by co-expression of a reporter gene, adenovirus expressing the mutant herpesviral thymidine kinase (HSV1-sr39tk) reporter gene and the human $VEGF_{121}$ gene independently in 2 expression cassettes ($Ad_{Tk\text{-}VEGF}$) (5) was applied in all 8 pigs. The injection site (basal or apical) was varied to control for interfering effects (Table 1). For injection into the second site, control adenovirus expressing only 1 transgene, either the HSV1-sr39tk reporter gene (Ad_{sr39tk}; n = 4), or the $VEGF_{121}$ gene (Ad_{VEGF}; n = 4), was used.

PET-CT imaging protocol. Imaging was done on a Siemens Biograph Sensation 16 scanner (Siemens Medical Solutions, Malvern, Pennsylvania), a hybrid system incorporating a 16-slice X-ray CT and a 3D LSO crystal-equipped PET component. [^{18}F]fluoro-hydroxymethylbutyl-guanine (FHBG) and [^{18}F]galacto-RGD were synthesized as previously described (6,7).

All animals were scanned in supine position under anesthesia with mechanical ventilation. Heart rate, blood oxygen saturation, and electrocardiogram were recorded continuously. Imaging sessions started with an X-ray topogram for orientation, followed by a low-dose CT (tube voltage 120 kV, tube current 14 mA) of the cardiac region for subsequent correction for photon attenuation. Ventilation was temporarily stopped for CT to obtain images in an intermediate breathing position for improved alignment between CT and PET.

Subsequently, PET emission data were obtained. Myocardial perfusion was assessed by use of [^{13}N]ammonia. At rest, 185 to 240 MBq were injected intravenously, and a 10-min dynamic acquisition in list mode, immediately followed by a static image of 10 min, was acquired. After a break of 30 min to allow for decay, pharmacologic vasodilation was induced by infusion of adenosine (0.14 mg/kg/min) for 5 minutes. Two minutes into the adenosine infusion, a second dose of [^{13}N]ammonia was injected and another set of images was obtained. In the 8 animals that received adenoviral vectors, 160 to 260 MBq of [^{18}F]FHBG were then injected, and a 20-min static image was obtained 45 min after injection.

After PET, the session was concluded with contrast-enhanced CT. Imaging of a test bolus of 20 ml contrast agent (Imeron300, Altana Pharma, Konstanz, Germany) was performed. Then mechanical respiration was stopped again, 70 ml contrast agent was injected at 4 ml/s, and a volume data set was acquired (tube voltage 100 kV, tube current 550 mA), covering the entire cardiac region with continuous electrocardiogram co-registration.

Four animals underwent a second PET-CT session at day 3 to 9 after surgery. This session consisted of CT, a [^{13}N]ammonia perfusion measurement at rest, as described

in the preceding, and injection of 170 to 215 MBq [^{18}F]galacto-RGD and a 30-min static image after 60 min.

PET data analysis. Attenuation-corrected transaxial images were reconstructed by an iterative algorithm (OSEM, 4 iterations, 8 subsets, 128 × 128 matrix, slice thickness 3 mm, no overlap). Using in-house-developed software (Munich Heart) (8), volumetric sampling was performed to identify 460 myocardial segments in the resting perfusion study of each session. For precise regional co-localization, segments were then transferred to images of stress perfusion and [^{18}F]FHBG and [^{18}F]galacto-RGD distribution. Polar maps of left ventricular myocardial uptake for each tracer were generated and normalized. Regional tracer uptake was expressed as percentage of the maximum in 9 myocardial areas (anterior, lateral, septal, and inferior wall, divided in basal and distal areas; apex as separate area). The 2 injection areas along with a remote area were defined according to the experimental protocol and according to localization of titanium clip markers at CT.

Absolute quantification of myocardial blood flow (MBF) was performed by use of dynamic [^{13}N]ammonia datasets, based on a validated three-compartment model (9). List mode data were rebinned to 18 consecutive dynamic image datasets (12 × 10 s, 4 × 60 s, 2 × 120 s). Arterial input function was defined by a small region of interest in left ventricular cavity. Motion-corrected time activity curves were extracted for the 460 myocardial segments previously defined from static images. The MBF in ml/g/min was calculated for each segment by compartment-model fitting and depicted in a polar map.

CT image analysis. For contrast-enhanced CT, overlapping transaxial images were reconstructed using a medium-smooth convolution kernel (B30f, 512 × 512 matrix, slice thickness 1 mm, increment 0.7 mm). Image reconstruction was retrospectively gated to the electrocardiogram. The reconstruction window was varied with a 10% increment, and 10 datasets covering the cardiac cycle in different phases were obtained. Artifact-free data sets were chosen for volume-rendered display and software-based overlay with PET. Data sets for all 10 phases were re-angulated perpendicular to the left ventricular long axis. Using in-house-developed software (Munich Heart), endocardial and epicardial contours were drawn in end-systolic and end-diastolic short-axis slices. The left ventricular ejection fraction (LVEF) was obtained, and regional end-diastolic and end-systolic wall thickness and thickening were calculated for clip-marked injection sites and a remote area in inferior wall. The

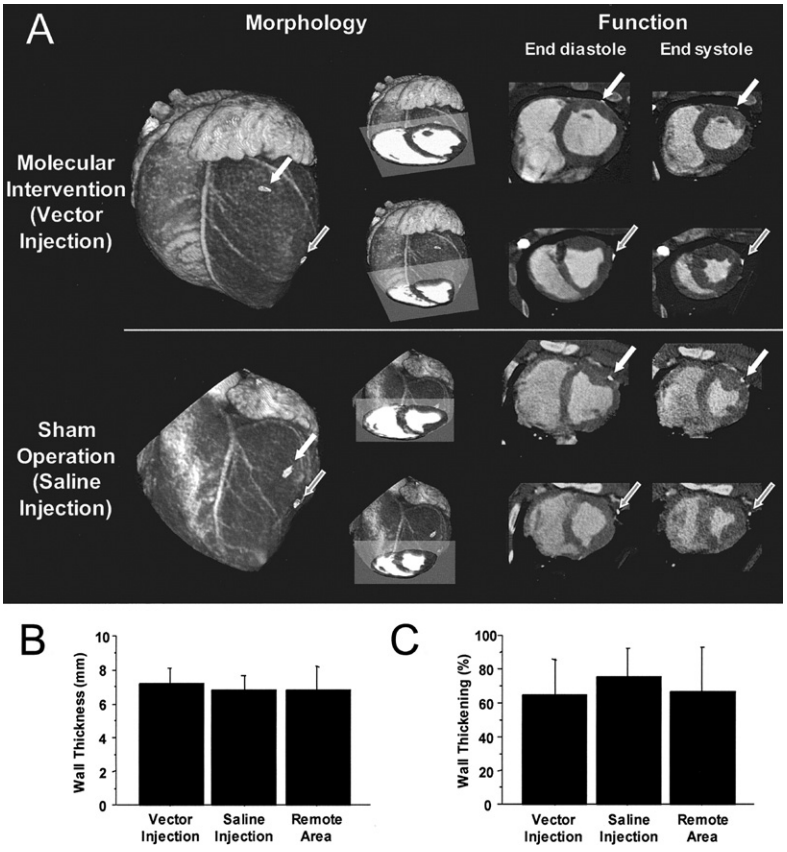

Figure 1. Assessment of morphology and contractile function. **(A)** Contrast-enhanced multislice computed tomographic (CT) images obtained during positron emission tomography–CT in an animal (animal 5; Table 1) after adenoviral gene transfer **(top)** and a control animal (animal 10; Table 1) after saline injection **(bottom)**. Surface-rendered images (**left**, anterior view) allow for accurate identification of clip-marked injection sites in basal anterior and distal anterolateral wall **(arrows)**. Ventricular function is determined from end-diastolic **(middle right)** and end-systolic short-axis images **(right)**. **(B and C)** Mean ± SD of regional end-diastolic wall thickness and thickening.

JACC Vol. 48, No. 10, 2006
November 21, 2006:2107–15

PET-CT fusion images were generated following manual readjustment, using standard software provided by the manufacturer.

Measurement of plasma VEGF concentration. Blood samples were taken before surgery and 6, 30, and 48 h after the surgical intervention. Plasma levels of human VEGF gene product were measured using a VEGF enzyme-linked immunosorbent assay kit (Calbiochem, Schwalbach, Germany).

Histology and immunohistochemistry. Formalin-fixed myocardial specimens were embedded in paraffin. For qualitative histologic examination of vascular/capillary density, paraffin sections (2 μm) were stained according to van Gieson. For immunohistochemistry, sections were deparaffinized, dehydrated, and pressure-cooked in citrate buffer, followed by blocking of endogenous peroxidase (3% H_2O_2/methanol).

Immunostaining for transgene products used streptavidin-horseradish-peroxidase technique with incubation of slides with polyclonal rabbit anti–HSV1-tk or anti-humanVEGF antibody and consecutively with ready-to-use anti-rabbit antibody (Dako ChemMate Detection Kit K5001; Dako-Cytomation, Hamburg, Germany).

Immunostaining for microvascular density used the APAAP technique (DAKO Chem Mate Detection Kit APAAP, Mouse). Primary antibody against alpha smooth muscle actin (DAKOCytomation Clone 1A4, 70 mg/l, 1:50 diluted) was used. For quantification, 10 high-power fields (HPF) from a representative slice of vector-injected regions were microscopically analyzed, and small vascular structures were counted.

Statistical analysis. Data were analyzed with StatView5.0 software (SAS Institute, Cary, North Carolina). Values are expressed as mean ± SD. Differences were assessed by paired/unpaired *t* test as appropriate or (for multiple comparisons) by 1-way analysis of variance with the Fisher penalized least square of differences post hoc test. A 2-sided p value of <0.05 was defined as significant.

RESULTS

CT identifies cardiac intervention sites and preserved structure and function. Titanium clip markings were reliably identified in all animals (Fig. 1A), allowing for fusion and co-localization with PET-derived biologic images. Global LVEF was normal in all animals. There was no difference between adenovirus-injected animals and saline-injected control animals (57 ± 5% vs. 53 ± 5%; p = 0.36). Consistently, regional contractile function was homogeneous. There was no difference for regional wall thickening between adenovirus-injected, saline-injected, or noninjected areas (p = 0.73) (Fig. 1C). Absolute end-diastolic wall thickness was also not different between regions (p = 0.70) (Fig. 1B).

PET reporter gene imaging and PET-CT image fusion identify successful gene transfer and regional transgene expression. All sites injected with adenoviral vector encoding for HSV1-sr39tk reporter gene ($Ad_{Tk\text{-}VEGF}$ or Ad_{sr39tk}) revealed significantly elevated uptake of FHBG compared with Ad_{VEGF}-injected or remote areas ($p < 0.01$) (Fig. 2A). Increased regional uptake co-localized with titanium clip markings (Figs. 3A and 3B). in vivo results were confirmed by ex vivo immunohistochemistry. Expression of HSV1-sr39tk gene product was identified in cytosol and nuclei of

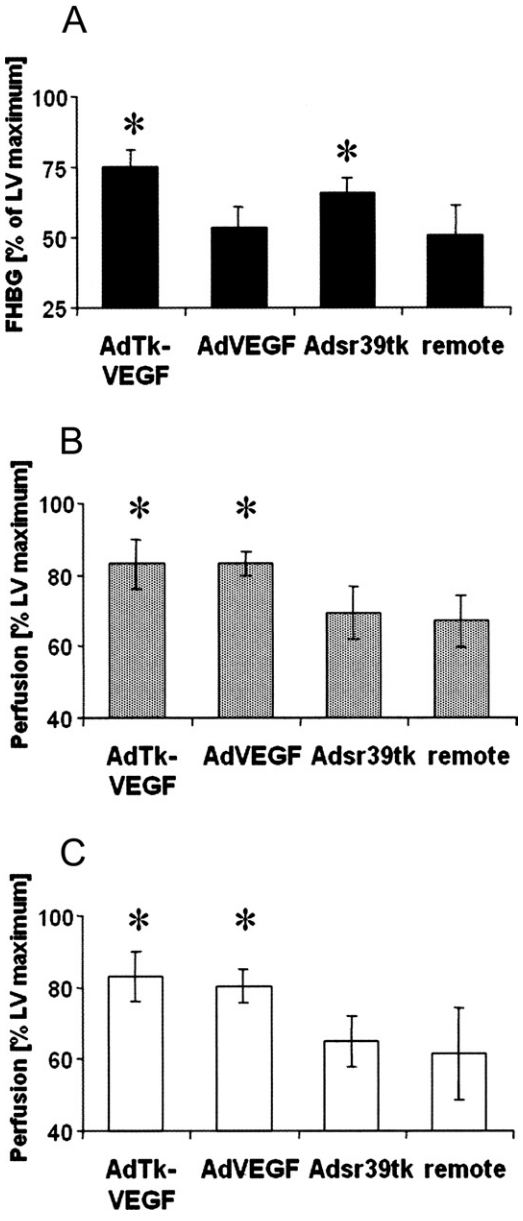

Figure 2. Uptake of tracers of myocardial reporter gene expression and perfusion in regions of adenoviral gene transfer ($Ad_{Tk\text{-}VEGF}$ [n = 8]; Ad_{VEGF} [n = 4]; Ad_{sr39tk} [n = 4]; remote [n = 8]). **(A)** Regional uptake of the reporter probe [^{18}F]fluoro-hydroxymethylbutyl-guanine (FHBG). *$p < 0.01$ vs. Ad_{VEGF} and remote. **(B)** Regional uptake of the perfusion tracer [^{13}N]ammonia at rest. *$p < 0.01$ vs. Ad_{sr39tk} and remote. **(C)** [^{13}N]ammonia uptake during adenosine vasodilation. *$p < 0.01$ vs. Ad_{sr39tk} and remote). **Bars** indicate mean ± SD.

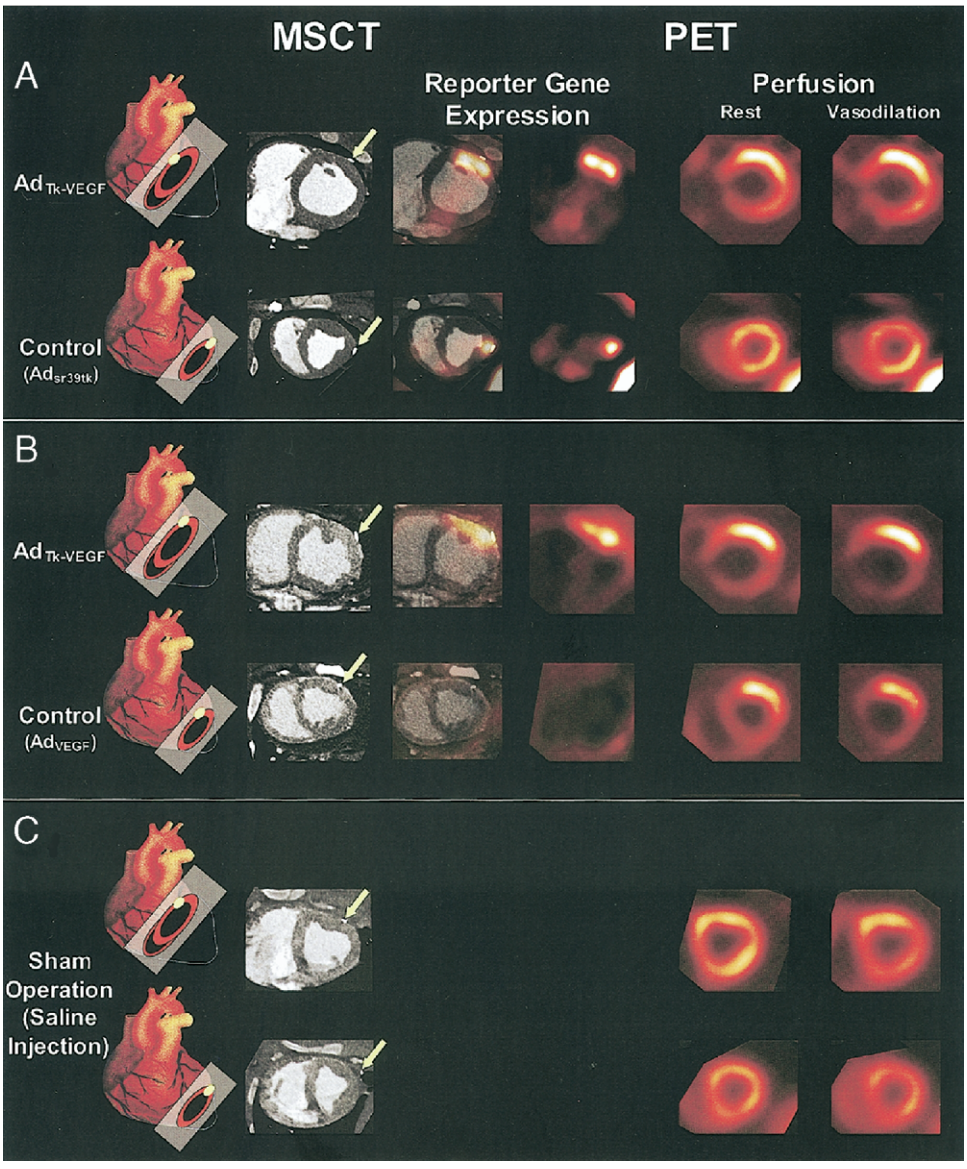

Figure 3. Positron emission tomography (PET)–computed tomographic (CT) imaging of morphology and biology. Representative short-axis tomographic images are shown. **(A)** Study animal (animal 1; Table 1) after regional injection of adenovirus carrying HSV1-sr39tk reporter gene together with $VEGF_{121}$ gene ($Ad_{Tk\text{-}VEGF}$, **top row**), or HSV1-sr39tk reporter gene only (Ad_{sr39tk}, **bottom row**). **(B)** Another study animal (animal 3; Table 1) after regional injection of $Ad_{Tk\text{-}VEGF}$ **(top row)**. This time, virus expressing $VEGF_{121}$ only was used as internal control (Ad_{VEGF}, **bottom row**). **(C)** Control animal (animal 9; Table 1) after regional injection of saline at both sites. Columns from **left to right**: on the left, a schematic display of individual location and orientation of short-axis slices, along with injection sites **(yellow)** is shown; next, contrast-enhanced multislice CT depicts location of titanium clip markings **(yellow arrows)**, along with circumferential wall thickness; next, PET-CT fusion of morphologic CT with PET images of the reporter probe [^{18}F]fluoro-hydroxymethylbutyl-guanine (FHBG) show significant accumulation of FHBG, colocalizing with clip markings in areas expressing the HSV1-sr39tk reporter gene (animal A, **both rows**; animal B, **top row**); on the right, PET perfusion images at rest and during adenosine-induced vasodilation show significantly elevated [^{13}N]ammonia uptake at sites where $VEGF_{121}$ is overexpressed (animal A, **top row**; animal B, **both rows**), whereas it is regionally homogeneous after Ad_{sr39tk} injection (animal A, **bottom row**) or saline injection (animal C).

myocardial cells in areas injected with $Ad_{Tk\text{-}VEGF}$ or Ad_{sr39tk}. Immunostaining for VEGF was positive in the cytosol of myocardial cells in areas injected with $Ad_{Tk\text{-}VEGF}$ or Ad_{VEGF} (Fig. 4).

Further support for successful transgene expression was obtained by the appearance of the secretable gene product $VEGF_{121}$ in the systemic circulation. Human VEGF was not detectable in saline-injected animals, nor was it detectable in blood samples before adenoviral injection. After gene transfer, the gene product appeared in the blood of all vector-injected animals, peaked (755 ± 946 pg/ml) at 6 h, declined (385 ± 783 pg/ml) by 30 h, and was detectable in only 1 animal at 48 h after gene transfer.

PET-CT identifies enhanced relative and absolute perfusion after VEGF gene transfer. There was a significant increase of relative uptake of [^{13}N]ammonia in VEGF-transduced areas after injection of either $Ad_{Tk\text{-}VEGF}$ or Ad_{VEGF} ($p < 0.01$ vs. Ad_{VEGF} and remote areas) (Figs. 2B, 2C, 3A, and 3B). No differences were found between Ad_{sr39tk}-injected and noninjected control areas. All saline-

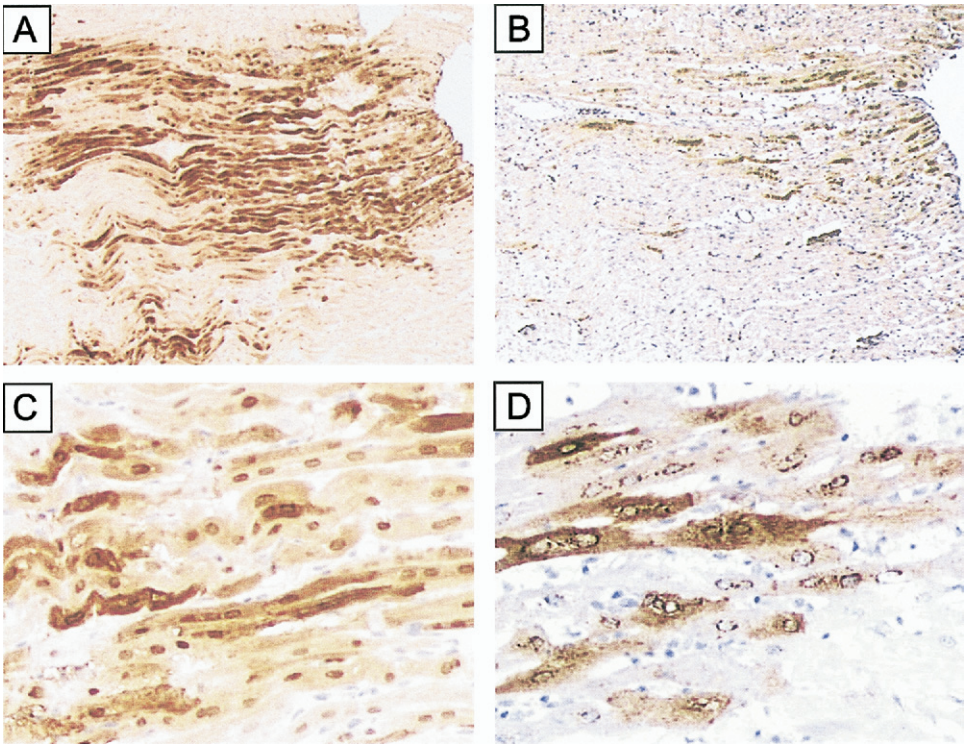

Figure 4. Ex vivo immunohistochemical staining of transgene products. Shown are microscopic images of a representative sample from a myocardial area injected with adenovirus carrying HSV1-sr39tk reporter gene together with the $VEGF_{121}$ gene ($Ad_{Tk\text{-}VEGF}$). Immunostaining for HSV1-tk **(A and C)** and VEGF **(B and D)** was performed in adjacent slices. **Dark brown color** indicates presence of the respective gene product. Low magnification **(A and B)** shows corresponding expression of both transgene products in the same tissue region. High magnification **(C and D)** identifies HSV1-tk reporter gene product in cytosol and nuclei, whereas VEGF is found in cytosol only, partly in a vesicle-like pattern. Subtle differences in strength and cellular localization of the immunostaining signal are explained by gene product characteristics (HSV1-TK is an intracellular enzyme, VEGF is a secretable substance).

injected control animals showed regionally homogeneous perfusion, ruling out procedure-related influences (Fig. 3C).

Because regionally increased relative uptake of [^{13}N]ammonia in static PET images may occur because of increased vascular permeability without a true increase of absolute tissue perfusion, we additionally explored quantitative MBF from dynamic images. At intraindividual comparison, MBF at rest in study animals was not significantly different between areas injected with $Ad_{Tk\text{-}VEGF}$ and remote areas (0.85 ± 0.22 vs. 0.78 ± 0.13 ml/g/min; $p = 0.19$). During adenosine vasodilation, MBF was significantly higher compared with remote areas (1.47 ± 0.49 vs. 1.14 ± 0.27 ml/g/min; $p = 0.01$). Overall, MBF in vector-injected animals was in the range of MBF measured in respective regions of sham-operated animals (0.75 ml/g/min at rest and 1.31 during adenosine), when compared interindividually.

Postmortem analysis revealed mildly, but significantly, enhanced microvascular density in areas injected with VEGF-expressing vector (5.57 ± 2.15 microvessels/HPF vs. 2.17 ± 1.11 for Ad_{sr39tk}-injected areas; $p = 0.03$) (Fig. 5).

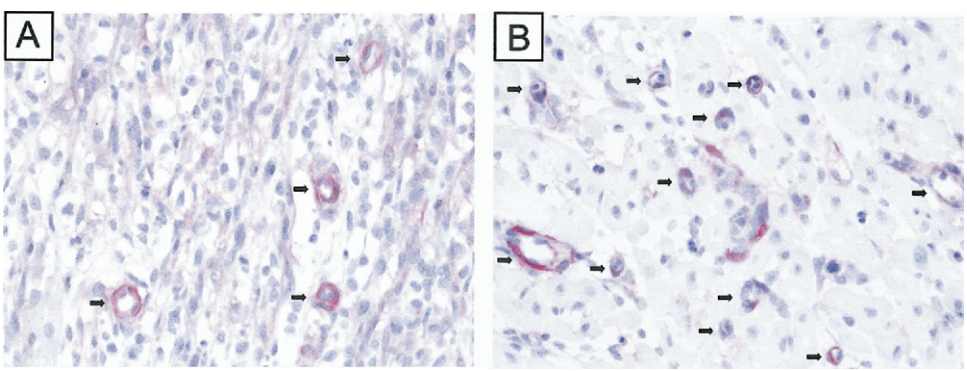

Figure 5. Ex vivo immunohistochemical staining of microvessels. **Pink** color indicates presence of smooth muscle actin (small vessels indicated by **arrows**). Shown are microscopic images of samples from a myocardial area injected with adenovirus carrying HSV1-sr39tk only (Ad_{sr39tk}) **(A)**, and of another area of the same animal injected with adenovirus carrying HSV1-sr39tk reporter gene together with the $VEGF_{121}$ gene ($Ad_{Tk\text{-}VEGF}$) **(B)**. Higher microvascular density is present in the VEGF-exposed area.

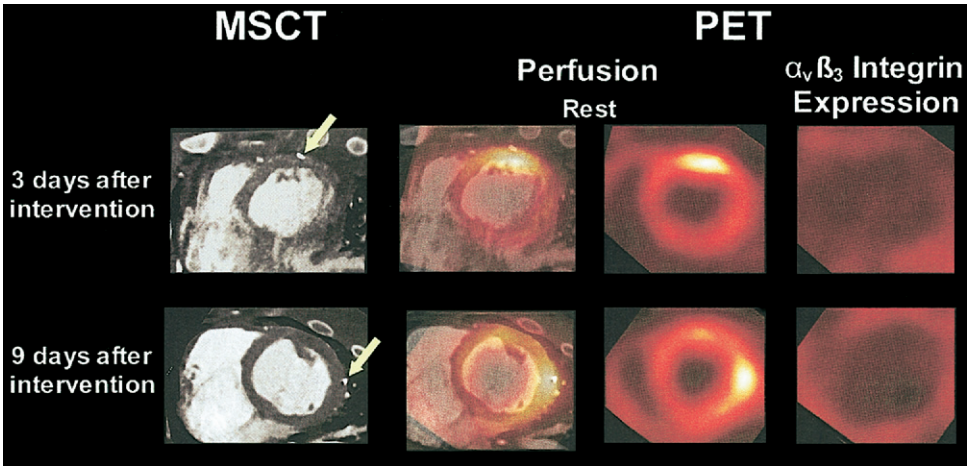

Figure 6. Positron emission tomography (PET)–computed tomographic (CT) imaging of integrin expression. Shown are representative short-axis slices through injection sites receiving adenovirus carrying the HSV1-sr39tk reporter gene together with the $VEGF_{121}$ gene ($Ad_{Tk\text{-}VEGF}$) in 2 different animals which underwent a repeat PET-CT session at 3 (**top**, animal 5; Table 1) or 9 (**bottom**, animal 7; Table 1) days after adenovirus injection. CT images (multislice computed tomography [MSCT], **left**) depict location of titanium clip markings of injection sites **(yellow arrows)**. **Middle left** shows fusion of MSCT with PET images of the perfusion tracer [^{13}N]ammonia at rest. PET perfusion images **(middle right)** show significant accumulation of [^{13}N]ammonia at the site of $Ad_{Tk\text{-}VEGF}$ injection. PET images of [^{18}F]-galacto-RGD **(right)** show no accumulation at vector injection sites.

VEGF-induced regional perfusion increase is not associated with up-regulation of $\alpha_v\beta_3$ integrin. The second PET-CT session at 3 to 9 days after the intervention focused on measurement of $\alpha_v\beta_3$ integrin expression. Perfusion tracer uptake was again measured at rest, and was still significantly elevated in regions overexpressing VEGF (80 ± 6% vs. 63 ± 8% in remote areas; $p = 0.002$), confirming persistence of vascular effects.

Overall myocardial uptake of the $\alpha_v\beta_3$ integrin-targeted tracer [^{18}F]-galacto-RGD was very low, and no focal uptake was detected in regions of VEGF overexpression showing increased perfusion (Fig. 6). Relative regional uptake was not different from remote areas (72 ± 5% vs. 75 ± 9%; $p = 0.45$).

DISCUSSION

In summary, the present study demonstrates that integrated PET-CT can be used to get detailed in vivo insights into biologic mechanisms of the heart. Changes induced by molecular intervention were characterized from gene expression over physiologic changes to morphologic appearance. Successful adenoviral transfer and subsequent expression of target gene ($VEGF_{121}$) in myocardium was specifically identified by PET imaging of a co-expressed reporter gene, which co-localized with clip-marked myocardial injection sites detected by CT. With the help of CT co-localization, specific effects of target gene overexpression on myocardial microcirculation at rest and during vasodilation were then characterized by quantitative perfusion imaging. The same technique also suggested that $\alpha_v\beta_3$ integrins do not play a role in the early phase of this VEGF-induced increase of myocardial perfusion in healthy myocardium. Finally, co-registration of CT further added to PET-determined biologic data by defining morphology and confirming absence of impairments of contractile function. These findings establish an imaging modality with substantial future potential in development and monitoring of cardiovascular therapy.

Integrated PET-CT has reportedly been useful for clinical imaging of myocardial perfusion and viability (10–13). The present study goes into further detail and demonstrates the feasibility of molecular characterization of the heart by integrating information from multiple PET tracers and contrast-enhanced CT. It is suggested that PET-CT has substantial potential as a translational tool that can be applied in experimental models as well as in clinical practice. For future clinical application, issues related to radiation exposure by combined nuclear and X-ray techniques need to be considered, and short-lived PET tracers will still require an on-site cyclotron for production. But it can be expected that localization and interpretation of the often weak specific signal from molecular-targeted PET probes will be facilitated by co-registration with high-resolution cardiac CT. Although fusion of PET and CT data had to be visually realigned in this study owing to potential influences of respiratory and cardiac motion, algorithms that allow for registration of respiratory motion during imaging are under development. These are expected to improve the precision of spatial co-registration in the future (14) and may help to circumvent problems with faulty attenuation correction of PET data from potentially misaligned CT scans to extend the application of PET-CT beyond myocardial imaging toward biomorphologic imaging of coronary vessels in the future.

Although proof of principle for the usefulness of PET-CT as a cardiac molecular imaging tool was the primary goal of this study, we chose a model of VEGF myocardial gene transfer, which allowed for using the novel imaging approach to get further insights into the mechanisms and consequences of VEGF overexpression. This

model was chosen because it has been considered promising for angiogenesis therapy of myocardial ischemia (2). Difficulties with this therapy were encountered when trying to reproduce experimental results in clinical trials (3,4), emphasizing the need for a more detailed understanding of therapeutic mechanisms and for more specific techniques to monitor success. To avoid the complexity and interindividual heterogeneity associated with animal models of myocardial ischemia, we chose for this initial methodologic evaluation to study effects of VEGF gene transfer in a stable model of surgical injection into healthy myocardium. Our results show that VEGF, when successfully overexpressed in normal heart muscle, increases regional myocardial perfusion. The CT morphology helped in accurately identifying the area of intervention and in localization of perfusion increase. It is tempting to speculate that lack of morphologic information to accurately identify injection sites may have resulted in a lack of observation of physiologic in vivo effects of gene transfer in a previous study with stand-alone microPET (15).

Interestingly, expression of $\alpha_v\beta_3$ integrins did not seem to play a role in the VEGF-induced increase of perfusion early after gene transfer in our study. $\alpha_v\beta_3$ Integrin is a group of adhesion molecules which has been targeted previously by molecular imaging as playing a role in post-myocardial infarction angiogenesis (16). The tracer used in the present study has been extensively validated as a marker of $\alpha_v\beta_3$ integrin expression in previous studies (7,17,18).

The sum of the effects of VEGF on healthy myocardium observed in the present study are most likely explained as follows. Our imaging studies were performed a few days after adenoviral gene transfer, at a time when expression of transgenes is known to be highest. Tissue levels of VEGF therefore reached a peak at this early time. Vascular endothelial growth factor is known to be a potent vasodilator, because it activates endothelial nitric oxide synthase and thus increases nitric oxide (NO) levels (19). Additionally, VEGF is known to increase vascular permeability through formation of intercellular gaps, vacuoles, and fenestrations, an effect partially mediated via NO release (20). The observed increase of perfusion at rest and during pharmacologic vasodilation is therefore most likely explained by these direct effects of overexpressed VEGF on the microvasculature. Vasodilation and increased microvascular denisty have also recently been established as important NO-mediated precursors of angiogenesis (21). Significant amounts of new blood vessel are not expected to have formed at this early time, and the mild increase of histologic microvascular density may be associated with vasodilation and thus improved detectability of microvessels. Expression of integrin adhesion molecules may not yet play a role or may require the strong stimulus of ischemic myocardial damage suggested in previous studies (16) for detectability, which was not present in our setup of healthy myocardium. Although this hypothesis for an underlying mechanism of our observations is at present speculative, it will be interesting to determine its validity in future molecular imaging studies of disease models. Notably, quantitatively assessed global microvascular reactivity was low (ratio stress/rest MBF >2) compared with values obtained in other animal and human studies. But this observation was true for vector-injected and sham-operated animals. It is therefore not specific for the molecular intervention and may rather be attributed to surgical or anesthetic procedure.

In conclusion, our study provides proof of feasibility for integrated multislice PET-CT to dissect cardiac biologic mechanisms following a molecular intervention. The technique seems ready for serial application in other animal models and models of cardiac disease or new therapies. Vascular endothelial growth factor gene transfer, or novel refined techniques for angiogenesis gene therapy (e.g., more complex models of short- and long-term ischemia) can be evaluated repetitively at different stages, and the obtained biologic and morphologic data may help in refining the clinical usefulness of therapy. Similarly, other molecular therapeutic approaches in the fields of cardiac gene therapy, cell transplantation, or tissue engineering can be evaluated noninvasively using this powerful biomorphologic imaging technique.

Acknowledgments

We thank the PET center, cyclotron unit, and animal care unit of TU München for assistance in radiotracer production, image acquisition, and animal handling.

Reprint requests and correspondence: Dr. Frank M. Bengel, Division of Nuclear Medicine, Russell H. Morgan Department of Radiology, Johns Hopkins University Medical Institutions, 601 N. Caroline Street, JHOC 3225, Baltimore, Maryland 21287. E-mail: fbengel1@jhmi.edu.

REFERENCES

1. Forrester JS, Price MJ, Makkar RR. Stem cell repair of infarcted myocardium: an overview for clinicians. Circulation 2003;108:1139–45.
2. Isner JM. Myocardial gene therapy. Nature 2002;415:234–9.
3. Grines CL, Watkins MW, Mahmarian JJ, et al. A randomized, double-blind, placebo-controlled trial of Ad5FGF-4 gene therapy and its effect on myocardial perfusion in patients with stable angina. J Am Coll Cardiol 2003;42:1339–47.
4. Kastrup J, Jorgensen E, Ruck A, et al. Direct intramyocardial plasmid vascular endothelial growth factor-A165 gene therapy in patients with stable severe angina pectoris. A randomized double-blind placebo-controlled study: the Euroinject One trial. J Am Coll Cardiol 2005; 45:982–8.
5. Anton M, Wittermann C, Haubner R, et al. Coexpression of herpesviral thymidine kinase reporter gene and VEGF gene for noninvasive monitoring of therapeutic gene transfer—an in vitro evaluation. J Nucl Med 2004;45:1743–6.
6. Miyagawa M, Anton M, Haubner R, et al. PET of cardiac transgene expression: comparison of 2 approaches based on herpesviral thymidine kinase reporter gene. J Nucl Med 2004;45:1917–23.
7. Haubner R, Kuhnast B, Mang C, et al. [18F]Galacto-RGD: synthesis, radiolabeling, metabolic stability, and radiation dose estimates. Bioconjug Chem 2004;15:61–9.
8. Nekolla SG, Miethaner C, Nguyen N, et al. Reproducibility of polar map generation and assessment of defect severity and extent assessment in myocardial perfusion imaging using positron emission tomography. Eur J Nucl Med 1998;25:1313–21.

9. Hutchins GD, Schwaiger M, Rosenspire KC, et al. Noninvasive quantification of regional blood flow in the human heart using N-13 ammonia and dynamic positron emission tomographic imaging. J Am Coll Cardiol 1990;15:1032–42.
10. Di Carli MF. Advances in positron emission tomography. J Nucl Cardiol 2004;11:719–32.
11. DiFilippo FP, Brunken RC. Do implanted pacemaker leads and ICD leads cause metal-related artifact in cardiac PET/CT? J Nucl Med 2005;46:436–43.
12. Koepfli P, Hany TF, Wyss CA, et al. CT attenuation correction for myocardial perfusion quantification using a PET/CT hybrid scanner. J Nucl Med 2004;45:537–42.
13. Namdar M, Hany TF, Koepfli P, et al. Integrated PET/CT for the assessment of coronary artery disease: a feasibility study. J Nucl Med 2005;46:930–5.
14. Nehmeh SA, Erdi YE, Pan T, et al. Four-dimensional (4D) PET/CT imaging of the thorax. Med Phys 2004;31:3179–86.
15. Wu JC, Chen IY, Wang Y, et al. Molecular imaging of the kinetics of vascular endothelial growth factor gene expression in ischemic myocardium. Circulation 2004;110:685–91.
16. Meoli DF, Sadeghi MM, Krassilnikova S, et al. Noninvasive imaging of myocardial angiogenesis following experimental myocardial infarction. J Clin Invest 2004;113:1684–91.
17. Haubner R, Weber WA, Beer AJ, et al. Noninvasive visualization of the activated alphavbeta3 integrin in cancer patients by positron emission tomography and [(18)F]galacto-RGD. PLoS Med 2005;2:e70.
18. Pichler BJ, Kneilling M, Haubner R, et al. Imaging of delayed-type hypersensitivity reaction by PET and 18F-galacto-RGD. J Nucl Med 2005;46:184–9.
19. Kroll J, Waltenberger J. A novel function of VEGF receptor-2 (KDR): rapid release of nitric oxide in response to VEGF-A stimulation in endothelial cells. Biochem Biophys Res Commun 1999;265:636–9.
20. Bates DO, Hillman NJ, Williams B, et al. Regulation of microvascular permeability by vascular endothelial growth factors. J Anat 2002;200:581–97.
21. You D, Waeckel L, Ebrahimian TG, et al. Increase in vascular permeability and vasodilation are critical for proangiogenic effects of stem cell therapy. Circulation 2006;114:328–38.